Magnetic Properties of Carboxylate-Bridged Ferromagnetic Copper(II) Chains Coupled by Cation−π Interactions

Antonio J. Costa-Filho,[†] Otaciro R. Nascimento,[†] Luis Ghivelder,[‡] and Rafael Calvo*[,§]

Instituto de Física de São Carlos, Universidade de São Paulo, CP 369, CEP 13560-970, São Carlos, SP, Brazil, Instituto de Física, Universidade Federal do Rio de Janeiro, CP 68528, Rio de Janeiro 21945, RJ, Brazil, and Departamento de Física, Facultad de Bioquímica y Ciencias Biológicas, Universidad Nacional del Litoral, and INTEC (CONICET-UNL), Güemes 3450, 3000 Santa Fe, Argentina

Received: December 20, 2000

The exchange interactions between copper ions in (L-tryptophyl-glycinato)copper(II), $C_{13}H_{13}CuN_3O_3$ (named Cu(II)Trp-Gly) are determined by ac magnetic susceptibility and dc magnetization measurements in powder samples, and by EPR measurements in single-crystal samples. The copper ions in this compound are arranged in two symmetry-related types of chains along the **b** axis. Neighbor coppers in a chain at 5.14 Å are connected by equatorial syn−anti carboxylate bridges, which transmit the intrachain exchange interactions. Indole rings of neighbor tryptophan residues at apical positions of the copper ions provide cation−π contacts that give rise to pathways supporting exchange interactions between the chains. The susceptibility and magnetization data obtained in the temperature range $1.8 < T < 100$ K, with applied dc magnetic fields (**B**) up to 9 T are explained assuming one-dimensional spin chains with ferromagnetic intrachain coupling $2J/k = 3.9 \pm 0.1$ K, calculated from the zero-field susceptibility. The magnetization and ac susceptibility with applied magnetic field calculated with this value agree qualitatively with the experimental results. Quantitative discrepancies between experimental and calculated ac susceptibility, observed at low T and intermediate **B** are attributed to anisotropies of the intra- and interchain interactions. The g factor and line width of the single EPR line observed were measured in single crystals at 9.5 and 35 GHz. The angular variation of the g factor is analyzed in terms of the electronic properties. The angular variation of the line width allows us to evaluate the interchain exchange interactions, $|2J'|/k = 0.061 \pm 0.002$ K. We discuss the values of J and J' in terms of the structures of the carboxylate bridges (J) and the cation−π interactions (J'). This is the first time that a small magnetic interaction transmitted through a cation−π interaction between a metal ion and an aromatic ring can be identified and evaluated.

Introduction

Carboxylate bridges are probably the best-studied paths for superexchange interactions. Antiferromagnetic (AFM) exchange was observed in copper acetate,[1] a binuclear complex in which four symmetry-related syn-syn acetate groups bridge two copper ions at 2.616 Å.[2] This is a strong AFM coupling ($2J/k = -215$ K)[3] transmitted through these bridges. This magnitude varies very little among compounds with similar geometries and distances.[4−7]

Ferromagnetic (FM) and AFM interactions transmitted through the less symmetric syn−anti carboxylate bridges have been reported in clustered and polymeric compounds.[8−16] As discussed by Colacio et al.,[10,15] the magnitude and even the sign of the exchange interaction strongly depend on the molecular and electronic structure of the bridge. Structural and magnetic studies on FM helix-like chains provided by syn−anti carboxylate bridges involving Cu(II) and different equatorial oxygen ligands were also reported by Colacio et al.[11,15,16] A common feature of these compounds is ligands acting as tridentate toward a copper ion, and as monodentate toward the next copper in the chain. From the point of view of molecular magnetism and from the biological implications of the electronic structure of the bridges,[17] the exchange coupling between metal ions connected by these syn−anti carboxylate bridges is an attractive problem for which more detailed experiments and analyses are needed. In addition, FM spin chains are of great interest, and experimental realizations are scarce. Their static magnetic properties[4,5,18−21] and the elemental magnetic excitations[22,23] offer a wide range of possibilities, depending on the anisotropy of the exchange interactions within the chains and on the interchain interactions.

Noncovalent intermolecular bonds play a major role in the structure and function of biological macromolecules.[24] Hydrogen bonds,[25,26] the stacking of aromatic rings,[27−29] and cation−π interactions[24,30−32] have been described. Their characterization is difficult, because in general, the effects of these weak bonds are mixed with those of stronger covalent interactions. In addition to providing a structural link, the bonds connecting ions or molecules with unpaired spins $\mathbf{S}_i$ and $\mathbf{S}_j$ may give rise to paths for exchange interactions

$$(H_{ex})_{ij} = -2J_{ij}\,\mathbf{S}_i\cdot\mathbf{S}_j \qquad (1)$$

between the unpaired spins.[33] The magnitude $2J_{ij}$ of this interaction is related to the geometry and electronic structure of the bond, and thus, its evaluation provides information that complements the structural characterization. In addition, it has

* Fax: (+54-342) 455-0944. E-mail: Rafael.Calvo@dfbioq.unl.edu.ar.
[†] Universidade de São Paulo.
[‡] Universidade Federal do Rio de Janeiro.
[§] Universidad Nacional del Litoral.

10.1021/jp0045742 CCC: $20.00
Published on Web 05/05/2001

been shown that the magnitudes of the exchange interactions in biomolecules allow estimating electron-transfer rates.[34] Thus, studies of specific molecular fragments as exchange paths may provide information about possible properties of these fragments as electron-transfer paths.

Metal−amino acid and metal−peptide complexes mimic some of the weak bonds that are important in proteins.[35,36] The small magnetic interactions transmitted through these weak bonds have been measured in several compounds using EPR, magnetic susceptibility, magnetization, and specific heat measurements.[37−44] Here we study the magnetic properties of (L-tryptophylglycinato)copper(II) [Cu(II)Trp-Gly]. The structure of this compound has been reported recently.[45] It displays helical copper chains where the copper ions are connected by syn−anti carboxylate bridges. These chains are interconnected by bridges containing cation−π contacts between the copper ion and the indole rings of tryptophan residues at its apical positions. The tryptophan large side chain generates steric distortions in the metal coordination[46] that may produce a closer resemblance of the situation in a macromolecule. We report dc magnetization and ac magnetic susceptibility measurements in Cu(II)Trp-Gly as a function of the applied dc magnetic field up to 9 T, from 1.8 to 300 K, and detailed single-crystal EPR measurements at 9.5 and 35 GHz. The behavior of the susceptibility and magnetization data is assigned to FM chains, and the data are used to evaluate the intrachain exchange couplings using a classical spin-chain model[18] and the high-temperature series expansion reported by Baker et al.[19] (see the review of Willet et al.[20] on FM chains). Intrachain couplings are assigned to the syn−anti carboxylate bridges. The EPR study of single-crystal samples indicates that the interchain couplings are provided by weak exchange interactions transmitted through the cation−π contacts. The magnitude $|2J'|$ of the interchain exchange interaction is determined by considering the phenomenon of exchange narrowing.[47−49] Such evaluation is *independent* of the calculation of the intrachain interaction. The general procedure is to obtain this value from the deviations of the magnetic (thermodynamic) data from the magnetic behavior expected for a linear chain. This is the first measurement of an exchange interaction transmitted through a cation−π contact between a metal ion and an aromatic ring.

Experimental Section

Synthesis and Crystallization of Cu(II)Trp-Gly. Single crystals of the title compound were obtained from a 1:1 stoichiometric reaction of Trp-Gly (Sigma Chemical Co.) and $CuCl_2$ in water solutions.[45] After several days of slow evaporation, dark blue crystals were obtained from the solutions at pH 5. The crystals were parallelepipeds of up to about $1 \times 0.5 \times 0.5$ mm, with the longest dimension along **a**, and the lateral faces being {011} planes (see Figure 1). Grinding small single crystals made powder samples for magnetic measurements.

Magnetic Measurements. The data were obtained using a commercial magnetometer (Quantum Design PPMS) in a powder sample of 30.5 ± 0.3 mg of Cu(II)Trp-Gly. dc magnetization measurements were performed as a function of temperature, *T*, for various fixed values of the static dc magnetic field between 0.1 and 9 T, and at fixed temperatures, as a function of the applied field within this range. The dc static susceptibility $\chi_o(T)$ was calculated from magnetization data obtained for a field of 0.1 T. The ac susceptibility measurements were performed using an applied ac magnetic field of 10^{-3} T, at 1 kHz, as a function of *T* between 1.8 and 120 K, with fixed values of the applied dc magnetic fields between 0 and 9 T. Real (χ') and imaginary (χ'') contributions to the ac susceptibility were simultaneously measured during the experiments.

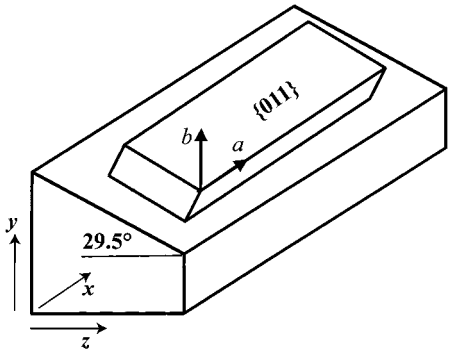

Figure 1. A typical single-crystal sample and its mounting for the EPR measurements.

EPR Measurements. EPR measurements were carried out at room temperature on single crystal samples using a Varian E-109 spectrometer working at 9.5 and 35 GHz and on cavities with 100 kHz field modulation. A Cu(II)Trp-Gly single crystal was mounted on a sample holder cut at a convenient angle such that the *a*, *b*, and *c* crystal axes were aligned along the *x*, *y*, and *z* laboratory reference system of the sample holder (Figure 1). The orientation of the magnetic field was varied by either using a goniometer (9.5 GHz) or rotating the electromagnet (35 GHz). The EPR measurements were performed with the magnetic field **B** in the three orthogonal crystal planes (*ab*, *ac*, *bc*). The line position and peak-to-peak line width (ΔB_{pp}) were obtained by least-squares fitting the digitally recorded spectra against a Lorentzian line shape.

Magnetic and EPR Results

dc Magnetization Measurements. The dc magnetization, *M*, was measured as a function of temperature, *T*, between 1.8 and 80 K for several values of the applied magnetic field; results between 1.8 and 60 K are shown in Figure 2A, where we plot the ratio between the observed value and the saturation value ($M_{sat} = 5770 \pm 5$ emu/mol) reached at high dc fields and low *T*. The dc magnetization was also measured as a function of the applied field, **B**, at six fixed temperatures; these results are shown in Figure 2B. No difference was observed between the $M(\mathbf{B})$ curves measured with increasing or decreasing magnetic field at the lowest temperature. The data in Figure 2A,B were corrected for the diamagnetic contribution using $\chi_{dia} = -1.55 \times 10^{-4}$ cm^3/mol, as calculated from standard Pascal constants.[5] From the saturation magnetization, we obtain an average *g* value of $g = 2.07(3)$. The uncertainty arises from the uncertainty in the mass of the sample.

ac Susceptibility Measurements. The values of the real part of the ac susceptibility χ' observed between 1.95 and 80 K at six fixed values of the applied dc magnetic field **B** from 0 to 9 T are shown in Figure 3A. Figure 3B displays the values of $T\chi'(T)$ as a function of *T*. All values in Figure 3A,B are corrected for diamagnetism as explained above. The values measured for the imaginary part χ'' of the ac susceptibility are 2 orders of magnitude smaller than those for the real part χ' and are not shown. The static susceptibility χ_o calculated from the magnetization data with a magnetic field of 0.1 T agrees within uncertainties with the values of the ac susceptibility at the same applied field. The observed agreement between $\chi_o(T)$ and $\chi'(T, B = 0.1\ \text{T})$, and the small values observed for χ'' support

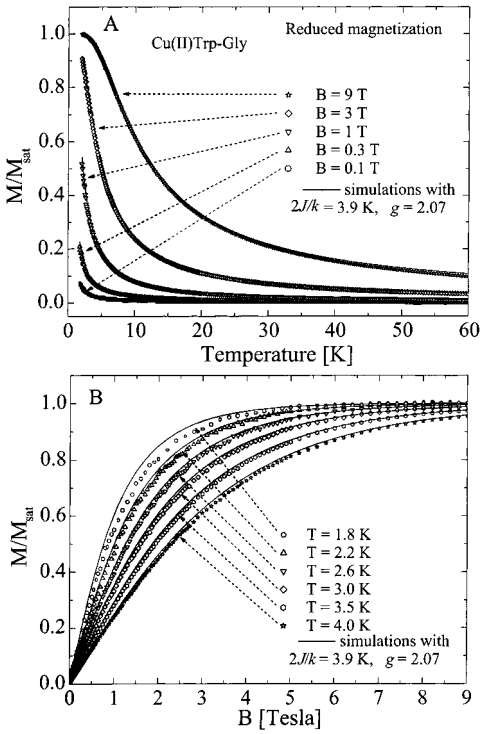

Figure 2. (A) Molar magnetization of a powder sample measured as a function of temperature for the indicated values of magnetic field. (B) Molar magnetization of a powder sample measured as a function of magnetic field at the indicated temperatures. The diamagnetic contribution to the data has been subtracted. Experimental data and simulations (see text) are included.

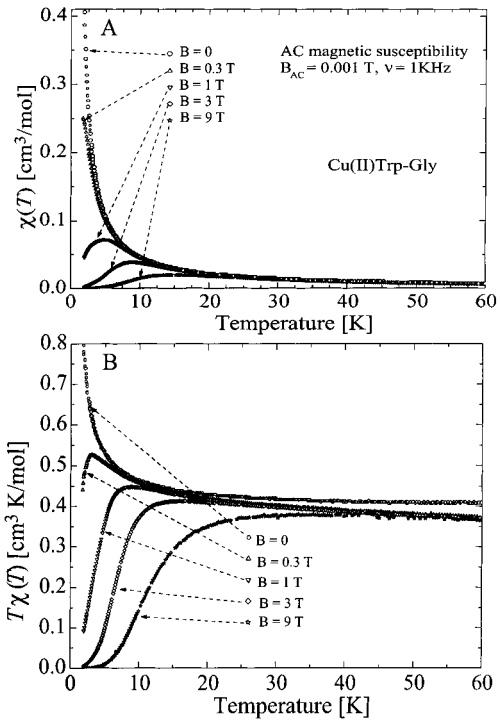

Figure 3. (A) Real part of the molar ac susceptibility, $\chi(T)$ vs T measured at the indicated applied dc magnetic fields, **B**, as a function of temperature. (B) Values of $T\chi(T)$ vs T obtained at the indicated values of **B**. Values measured at $B = 0.1$ T are not included to avoid cluttering of the figures. The diamagnetic contribution has been subtracted (see text).

neglecting the imaginary contribution to the ac susceptibility. Thus, we will refer to $\chi = dM/dB$, neglecting any out-of-phase contribution. The ac results for $\chi(T)$ measured with $B = 0$ between 1.8 and 80 K are displayed in Figure 4, which also includes a Curie plot. A fit of the Curie−Weiss equation,[4]

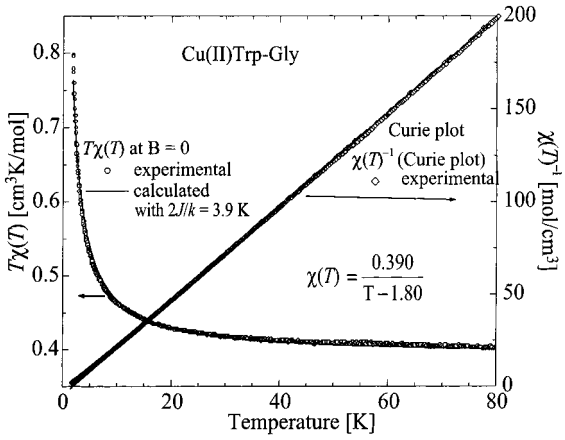

Figure 4. Left side: $T\chi(T)$ vs T, experimental and simulation (solid line) with eqs 9 or 12 using $2J/k = 3.9$ K. Right side: $\chi(T)^{-1}$ vs T (Curie Plot), experimental and fit with Curie−Weiss law. $\chi(T)$ is the real part of the molar ac magnetic susceptibility. Data are corrected for diamagnetism (see text). The values of the dc magnetic susceptibility calculated from magnetization data obtained at a field of 0.1 T agree within experimental accuracy with the ac results.

$$\chi(T) = \frac{C}{T - \Theta} \tag{2}$$

to the data in Figure 4 gives $C = 0.390 \pm 0.006$ emu/mol and $\Theta = (1.80 \pm 0.05$ K. This value of C gives $g = 2.04 \pm 0.02$ for the average g value of the copper ions. The sign of Θ reflects a FM interaction between neighbor coppers. Using the equation[4]

$$\theta = \frac{2zJS(S+1)}{3k} \tag{3}$$

($S = {}^1/_2$ for copper ions) and considering the two nearest copper neighbors in the chain ($z = 2$), we estimate $2J/k \approx 3.6$ K for the isotropic FM interaction ($2J$ defined in eq 1).

EPR Measurements. A single resonance for the four magnetically nonequivalent copper ions in the structure of Cu(II)Trp-Gly was observed in single-crystal samples. Its position and width were measured as a function of the magnetic field at 5° intervals in the *ab*, *cb*, and *ca* crystal planes. Figures 5 and 6 display the observed angular variation of the squared g factor and the peak-to-peak line width ΔB_{pp}, respectively, that are observed in these planes at 9.5 and 35 GHz and room temperature.

Crystal Structure of Cu(II)Trp-Gly and Possible Exchange Pathways. The structure of Cu(II)Trp-Gly ($C_{13}H_{13}CuN_3O_3$) has been reported.[45] It is orthorhombic, space group $P2_12_12_1$, with $a = 8.2829(5)$ Å, $b = 9.347(2)$ Å, and $c = 16.499(2)$ Å, and $Z = 4$. Figure 7A is a projection of the compound showing the atom numbering scheme. The copper ion is coordinated by one oxygen atom (O2), and two nitrogen atoms (N1 and N2) of one dipeptide, and by another oxygen atom (O1) of a symmetry-related dipeptide molecule. Thus, each peptide molecule acts as a tridentate ligand (through N1, N2, and O2) toward one copper ion and as a monodentate ligand (through O1) toward another copper ion. This results in a helical chain structure along the **b** axis where neighbor copper ions at 5.14 Å are connected by syn−anti carboxylate bridges between equatorial oxygen ligands (Figure 7B). This chain structure is

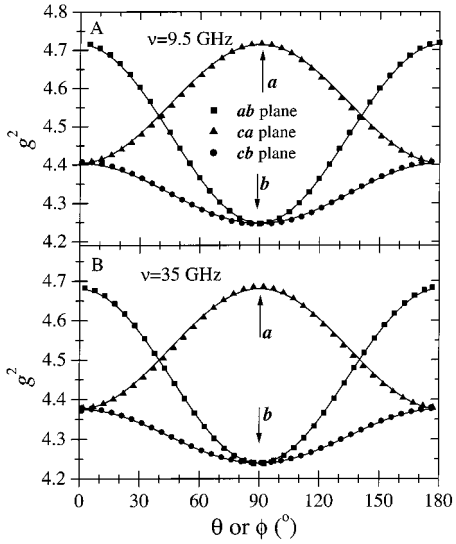

Figure 5. Experimental values of the $\mathbf{g}^2$ tensor for the single resonance observed at (A) 9.5 and (B) 35 GHz in the three crystallographic planes of a Cu(II)Trp-Gly single crystal. The solid lines were obtained using the components of $\mathbf{g}^2$ given in Table 1.

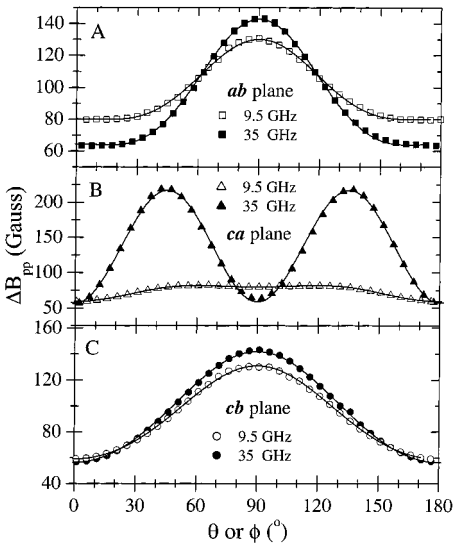

Figure 6. Experimental values of the peak-to-peak line width (ΔB_{pp}) in the three crystallographic planes of a Cu(II)Trp-Gly single crystal, at 9.5 and 35 GHz. The solid lines were obtained using eq 25 and the parameters in Table 2.

further stabilized by a hydrogen bond between the carbonyl oxygen (O3) of one dipeptide, and a nitrogen (N3) of the indole ring of the neighbor tryptophan ligand. The Cu(II) coordination is essentially square-planar with the copper ion displaced 0.063(1) Å from the mean-square plane of coordinated atoms. In addition, there are two indole rings of neighbor peptide molecules at the two apical positions.

The four rotated Cu(II) ions per asymmetric unit cell of Cu(II)Trp-Gly (labeled A, B, C, D) with fractional coordinates[50] (x, y, z), ($-x + {}^1/_2$, $-y$, $z + {}^1/_2$), ($-x$, $y + {}^1/_2$, $-z + {}^1/_2$), ($x + {}^1/_2$, $-y + {}^1/_2$, $-z$), are chemically equal, but magnetically nonequivalent in the presence of a magnetic field. The exchange pathways connecting neighbor copper ions are called paths A−A, A−B, A−C, and A−D. Two A atoms at $d(Cu^A-Cu^A) = 9.347$ Å along the b axis are connected by a path involving a row of 10 diamagnetic atoms, including the hydrogen bond mentioned above. The path Cu^A-Cu^A between coppers separated by $a = 8.2829$ Å is even more complex because pairs of Cu^A atoms have a Cu^B atom between them. Thus, the magnitude

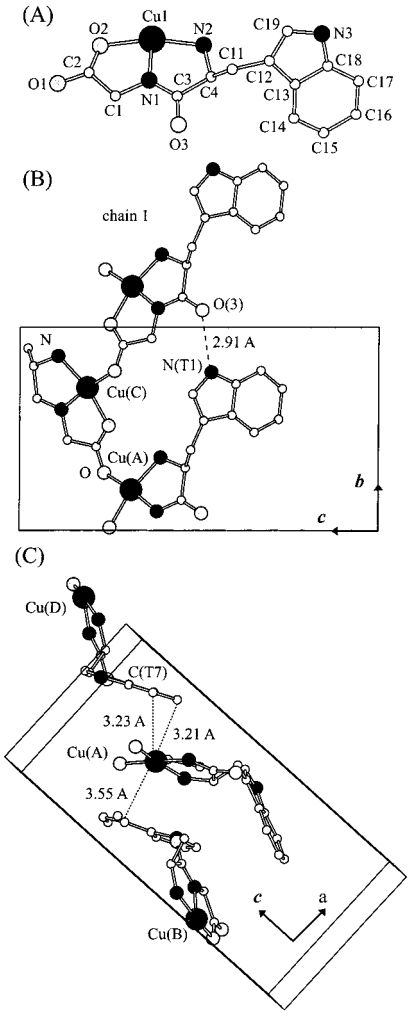

Figure 7. (A) Projection of the Cu(II)Trp-Gly molecule showing the labeling of the atoms. (B) Projection down the a axis displays the contacts A−C mediated by syn−anti carboxylate bridges. (C) View of the crystal down the **b** axis. The cation−π interactions between the copper ion and the indole rings at the two apical positions are emphasized (see text for description).

of the superexchange interaction through these A−A bridges is expected to be negligible. The contact A−B [two nearest copper neighbors at $d(Cu^A-Cu^B) = 7.53$ Å] is provided by a cation−π interaction between the electronic cloud of the copper ion and the π electron orbital of an indole ring plus the σ skeleton of the peptide. The shortest distance between the copper ion and the indole carbon atoms is $d(Cu^A-C14^B) = 3.55$ Å. The angle between the normal to the plane of the ring and the normal to the copper coordination plane is 15.4°. The contact Cu^A-Cu^C (two nearest copper neighbors related by a C_2 operation around b, at $d(Cu^A-Cu^C) = 5.14$ Å) is a covalent syn−anti carboxylate bridge ($Cu^A-O1^A-C2^C-O2^C-Cu^C$) (Figure 7B) where both oxygen atoms are equatorial ligands to copper. The copper ions are on the same side of the plane defined by the O1C2O2 carboxylate group, at 0.13 and 0.43 Å of the plane.The contact A−D (two nearest copper neighbors at $d(Cu^A-Cu^D) = 10.53$ Å) is also provided by a path containing a cation−π interaction, in this case through the indole ring at the opposite apical position, plus the σ skeleton of the peptide. The shortest distances involved in this cation−π contact are $d(Cu^A-C16^D) = 3.21$ Å and $d(Cu^A-C17^D) = 3.23$ Å (Figure 7C). The angle between the normal to the plane of the ring and the normal to the copper coordination plane is 22°. The copper displacement from the coordination plane is toward this indole

ring. The structure of this path (Figure 7C) suggests that the cation−π interaction of a copper-type A with the indole ring belonging to the neighbor molecule D may be stronger than the one involving pairs A−B of molecules. Superexchange interactions may be transmitted through A−B, A−C, A−D, and other symmetry-related paths. Undoubtely, those transmitted through the covalent carboxylate bridges (A−C and B−D paths) provide the strongest couplings, giving rise to a chain structure along the **b** axis. The relative strengths of the exchange interactions through the paths described above divide the copper ions in magnetic chains type 1, containing coppers A and C, and type 2, containing coppers B and D. The A−C contacts provide the intrachain interaction ($J = J^{(A,C)} = J^{(B,D)}$). The A−B and A−D contacts (and the symmetry-related B−C and C−D contacts) provide the interchain interaction (J'). From the magnetic point of view, these couplings interconnect the chains and tend to produce a three-dimensional magnetic structure.

Theory

To explain the magnetization and susceptibility data, we propose for Cu(II)Trp-Gly a linear spin-chain behavior with intrachain exchange coupling, J, which considers the structural information discussed above. The magnetic properties of the chains are calculated using a classical spin-chain model[18] that allows us to calculate the susceptibility and magnetization as a function of temperature and applied magnetic field **B**. We also used the high-temperature approximation of Baker et al.[19] for the magnetic susceptibility of a FM spin chain at $B = 0$. The spin chains are coupled by weaker interchain exchange couplings, J', that are not considered in the quantitative analysis of the magnetic data but are evaluated later from the single-crystal EPR data.

Magnetic Susceptibility and Magnetization of Isotropic Linear Chains. In the presence of a magnetic field **B**, isolated spin chains are described by the Hamiltonian[33]

$$H = -2J\sum_i S_i \cdot S_{i+1} + g\mu_B \sum_i S_i \cdot \mathbf{B} \tag{4}$$

Equation 4 assumes an isotropic exchange of magnitude $2J$ between nearest copper neighbors, an isotropic g factor (i.e., an average value, appropriate for a powder sample), and μ_B is the Bohr magneton. The molar magnetization observed for a magnetic field **B** applied along the ***z*** direction can be written as

$$M(\mathbf{B},T) = -\frac{N_o g \mu_B \langle S_z \rangle}{N_S} \tag{5}$$

and using eq 5, it is obtained for the molar magnetic susceptibility

$$\chi(\mathbf{B},T) = \frac{\partial M(\mathbf{B},T)}{\partial \mathbf{B}} = \frac{N_o g^2 \mu_B{}^2}{N_S\, kT}\,[\langle S_z{}^2\rangle - \langle S_z\rangle^2] \tag{6}$$

In eqs 5 and 6, N_o is the Avodagro's number, $\langle S_z\rangle$ and $\langle S_z{}^2\rangle$ are the thermal averages of S_z and $S_z{}^2$ calculated for a N_S spin chain in a field **B**, at the temperature T. Following Bonner and Fisher (BF)[18] we calculate $\langle S_z\rangle$ and $\langle S_z{}^2\rangle$ using the eigenvalues of finite chains with different N_S, and extrapolate the results to $N_S \rightarrow \infty$

$$\langle S_z\rangle = \frac{\sum_{i=1}^{n} S_{zi} \exp(-JE_i/kT)}{\sum_{i=1}^{n} \exp(-JE_i/kT)}$$

$$\langle S_z{}^2\rangle = \frac{\sum_{i=1}^{n} S_{zi}{}^2 \exp(-JE_i/kT)}{\sum_{i=1}^{n} \exp(-JE_i/kT)} \tag{7}$$

where $n = 2^{N_S}$ is the number of states of the chain, and

$$E_i = E_{io} + (g\mu_B B/J)S_{zi} = E_{io} + yS_{zi} \tag{8}$$

are the eigenvalues of an N_S spin chain in the field **B**, in units of J. We introduce in eq 8 the reduced magnetic field $y = g\mu_B B/J$. When $B = 0$, $\langle S_z\rangle$ is zero, and we get from eq 6 the usual expression for the molar static magnetic susceptibility $\chi_o(T)$.[4] Considering the information provided by the Curie plot (Figure 4), we discuss the data in terms of FM interactions. The energy levels E_{io} of the chain in the absence of an applied magnetic field (see eq 8) are defined with the multiplet having largest S_z ($S_z = N_S/2$) as the ground state. Defining the "reduced temperature" $x = kT/J$ (with $J > 0$, as for FM chains in eq 1), eq 6 can be written in terms of g, J, x, and y as

$$\chi(g,J,x,y) = W(g,J)\,\kappa(x,y) \tag{9}$$

that divides the susceptibility into two factors.

$$W(g,J) = N_o g^2 \mu_B{}^2/J \tag{10}$$

is a multiplicative factor that depends on the two physical parameters (g and $2J$) and describes the properties of the chain. The other factor,

$$\kappa(x,\mathbf{y}) = \frac{1}{xN_S}[\langle S_z{}^2\rangle - \langle S_z\rangle^2] \tag{11}$$

is the "reduced susceptibility", describing the shape of the variation of the chain susceptibility with reduced temperature (x) and magnetic field (**y**). It is also a function of the isotropic g factor, and the intrachain exchange parameter $2J$.

The results of BF[18] for the susceptibility of AFM chains in the case of $B = 0$ have been widely used to fit experimental results. FM chains were also analyzed by BF, but these results have received less attention because experimental realizations are less common.[5,18] In the analysis of our susceptibility and magnetization data with $B = 0$ and with $B \neq 0$, we used eqs 5 and 9 with the eigenvalues of chains of 11−16 spins. A limiting value of $\kappa(x,\mathbf{y})$ is approached uniformly for increasing values of N_S; the differences between the results for 14, 15, and 16 spin chains are negligible in the temperature range of interest, and thus, the result for 14 spins was used as the limiting value.

Colacio et al.[10,15] and other authors[5] analyzed data for FM chains[18] using the high-temperature expansion reported by Baker et al.,[19] valid for $B = 0$, which gives for the susceptibility at $B = 0$

$$\chi(T) = \frac{N_o g^2 \mu_B{}^2}{4kT} F(z) \tag{12a}$$

with $z = J/2kT$, and

$$F(z) = \left[\frac{1 + 5.7979916z + 16.902653z^2 + 29.376885z^3 + 29.832959z^4 + 14.036918z^5}{1 + 2.79799916z + 7.0086780z^2 + 8.6538644z^3 + 4.5743114z^4}\right]^{2/3} \quad (12b)$$

For $B \neq 0$, only eq 9 can be used.

Interchain Exchange Couplings and the Single-Crystal EPR Data. We analyzed the single-crystal EPR data in terms of the theory of Kubo and Tomita,[48] as described by Passeggi and Calvo.[49] The magnetic system is described by the spin Hamiltonian

$$H_s = H_z + H_{ex} \quad (13)$$

where H_z and H_{ex} are the Zeeman and exchange interactions. Hyperfine couplings are not important for our purpose. H_z is given by

$$H_z = \mu_B \sum_{i,\alpha} (\mathbf{S}_{i\alpha} \cdot \mathbf{g}_\alpha \cdot \mathbf{B}) = \mu_B \mathbf{S} \cdot \mathbf{g} \cdot \mathbf{B} + (\mu_B \sum_{u=1}^{3} \mathbf{s}_u \cdot \mathbf{G}_u \cdot \mathbf{B}) \quad (14)$$

where the index i runs over all of the crystal cells, $\mathbf{B}$ is the applied magnetic field, μ_B is the Bohr magneton, and $\mathbf{S}_{i\alpha}$ is the spin of the copper ion α (α = A, B, C, D) of the ith unit cell. $\mathbf{S}$ and $\mathbf{g}$ are the total spin and the average $\mathbf{g}$ tensor

$$\mathbf{S} = \sum_i (\mathbf{S}_{iA} + \mathbf{S}_{iB} + \mathbf{S}_{iC} + \mathbf{S}_{iD}) \quad (15)$$

$$\mathbf{g} = {}^1/_4(\mathbf{g}_A + \mathbf{g}_B + \mathbf{g}_C + \mathbf{g}_D) \quad (16)$$

Considering the symmetry of the $P2_12_12_1$ space group, the spin operators $\mathbf{s}_u$ and the tensors $\mathbf{G}_u$ are defined as

$$\mathbf{s}_1 = \sum_i (-\mathbf{S}_{iA} + \mathbf{S}_{iB} + \mathbf{S}_{iC} - \mathbf{S}_{iD})$$
$$\mathbf{s}_2 = \sum_i (\mathbf{S}_{iA} - \mathbf{S}_{iB} + \mathbf{S}_{iC} - \mathbf{S}_{iD})$$
$$\mathbf{s}_3 = \sum_i (\mathbf{S}_{iA} + \mathbf{S}_{iB} - \mathbf{S}_{iC} - \mathbf{S}_{iD}) \quad (17)$$

$$\mathbf{G}_1 = {}^1/_4(-\mathbf{g}_A + \mathbf{g}_B + \mathbf{g}_C - \mathbf{g}_D)$$
$$\mathbf{G}_2 = {}^1/_4(\mathbf{g}_A - \mathbf{g}_B + \mathbf{g}_C - \mathbf{g}_D)$$
$$\mathbf{G}_3 = {}^1/_4(\mathbf{g}_A + \mathbf{g}_B - \mathbf{g}_C - \mathbf{g}_D) \quad (18)$$

Equation 14 considers explicitly the anisotropy of the four symmetry-related $\mathbf{g}$ tensors, which was neglected in eq 4, used to explain the magnetization data in a powder sample. Because in our experiments a single exchange-collapsed resonance is observed in the three crystallographic planes (see Figure 5), the spin Hamiltonian can be written for a perturbative calculation as

$$H_s = H_o + H_1 \quad (19)$$

where

$$H_o = \mu_B S \cdot \mathbf{g} \cdot \mathbf{B} + H_{ex} \quad (20)$$

and

$$H_1 = \mu_B \sum_{u=1}^{3} \mathbf{s}_u \cdot \mathbf{G}_u \cdot \mathbf{B} \quad (21)$$

The exchange interaction H_{ex} is the sum of the contributions over the pairs of copper ions. Because the exchange interactions commute with the total spin S (eq 15), the result of H_o is a single resonance with the average g factor (eq 16). In the absence of exchange interactions, the residual Zeeman terms H_1 (eq 21) would split the resonances corresponding to the four copper sites. The exchange interaction term in H_o modulates H_1 and averages it to zero, producing the collapse of those four resonances; however, it still produces a broadening with a peak-to-peak line width ΔB_{pp} given by[49]

$$\Delta B_{pp}(\theta,\varphi) = \sqrt{\frac{2\pi}{3}} \frac{\omega_o{}^2 \hbar}{g\mu_B} \sum_{u=1}^{3} \frac{1}{\omega_{ex}^{(u)}} \frac{(\mathbf{h}\cdot\mathbf{g}\cdot\mathbf{G}_u\cdot\mathbf{h})^2}{g^4(\theta,\varphi)} \quad (22)$$

that depends on the squared microwave frequency ($\omega_o{}^2$), on the $\mathbf{g}$ and $\mathbf{G}_u$ tensors of eq 18 and on the orientation $\mathbf{h} = \mathbf{B}/|\mathbf{B}|$ of the external magnetic field. The $\omega_{ex}^{(u)}$ is the exchange frequencies that in the nearest neighbor approximation are given by[49]

$$(\omega_{ex}^{(1)})^2 = \frac{2}{\hbar^2}[(2J^{(A,B)})^2 + (2J^{(A,C)})^2] \quad (23a)$$

$$(\omega_{ex}^{(2)})^2 = \frac{2}{\hbar^2}[(2J^{(A,B)})^2 + (2J^{(A,D)})^2] \quad (23b)$$

$$(\omega_{ex}^{(3)})^2 = \frac{2}{\hbar^2}[(2J^{(A,C)})^2 + (2J^{(A,D)})^2] \quad (23c)$$

where we take into account the factor 2 in eq 1. These exchange frequencies can be evaluated from the fit of eq 22 to line width data in three orthogonal planes. Because in the bc plane $\mathbf{g}_A = \mathbf{g}_D$ and $\mathbf{g}_B = \mathbf{g}_C$, the only nonzero contribution is

$$(\mathbf{h}\cdot\mathbf{g}\cdot\mathbf{G}_1\cdot\mathbf{h})^2/g^2(\theta,\phi) \approx \{\mathbf{h}\cdot[{}^1/_2(-\mathbf{g}_A + \mathbf{g}_B)]\cdot\mathbf{h}\}^2 = g_{yz}{}^2 \sin^2\theta \cos^2\theta \quad (24a)$$

In the ac plane, $\mathbf{g}_A = \mathbf{g}_C$ and $\mathbf{g}_B = \mathbf{g}_D$, thus yielding the contribution

$$(\mathbf{h}\cdot\mathbf{g}\cdot\mathbf{G}_2\cdot\mathbf{h})^2/g^2(\theta,\phi) \approx \{\mathbf{h}\cdot[{}^1/_2(\mathbf{g}_A - \mathbf{g}_B)]\cdot\mathbf{h}\}^2 = g_{xz}{}^2 \sin^2\theta \cos^2\theta \quad (24b)$$

and in the ab plane, $\mathbf{g}_A = \mathbf{g}_B$ and $\mathbf{g}_C = \mathbf{g}_D$ the contribution is

$$(\mathbf{h}\cdot\mathbf{g}\cdot\mathbf{G}_3\cdot\mathbf{h})^2/g^2(\theta,\phi) \approx \{\mathbf{h}\cdot[{}^1/_2(\mathbf{g}_A - \mathbf{g}_C)]\cdot\mathbf{h}\}^2 = g_{xy}{}^2 \sin^2\phi \cos^2\phi \quad (24c)$$

Each $(\mathbf{h}\cdot\mathbf{g}\cdot\mathbf{G}_u\cdot\mathbf{h})^2/g^2(\theta,\phi)$ (u =1, 2, 3) is proportional to one nondiagonal matrix element of $\mathbf{g}_A$, $\mathbf{g}_B$, $\mathbf{g}_C$, and $\mathbf{g}_D$ in the crystal axes system. These components have to be calculated in order to use eq 22.

Analysis of the Data

Magnetic Susceptibility and Magnetization Data. Values of g and $2J$ were obtained by least-squares fitting the product $T\chi(T)$, calculated with eq 9 at $B = 0$, to the experimental results in Figure 3. Fitting $T\chi(T)$ is more sensitive to g and $2J$ and

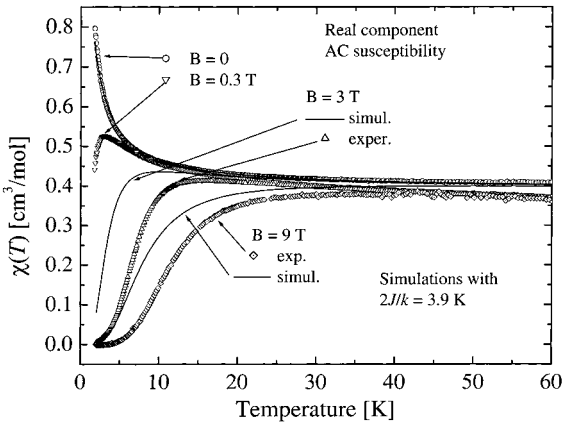

Figure 8. $T\chi(T)$ (real part of the ac susceptibility) as a function of temperature for four values of the applied dc magnetic field. The lines are the simulations performed with the model (see text). Severe disagreement between simulations and data is obtained for intermediate (nonsaturating) values of the magnetic field at the lowest temperatures.

gives better accuracy than fitting $\chi(T)$. This simple two-parameter model gives an excellent fit to the susceptibility data with $B = 0$ for $g = 2.04 \pm 0.02$ and $2J/k = 3.9 \pm 0.1$ K. The calculated values of $T\chi(T)$ are included as solid lines in Figure 4. In the case of $B = 0$, eqs 9 and 12 give results differing by $<0.1\%$ above $x > 0.25$, and they can be used indistinctly in the process of fitting. For $B \neq 0$, eq 12 is no longer valid, and we must use eqs 5 and 9 for calculating the magnetization and susceptibility. Hence, using these equations and the values of g and $2J$ given above, we calculated the magnetization and susceptibility as a function of temperature and the applied magnetic field. The predictions of the model for the reduced magnetization M/M_{sat} are shown in Figure 2A,B. The agreement is acceptable, showing small differences at the lowest temperature and in the intermediate field range between 1 and 4 T (see data points and calculated line corresponding to $T = 1.8$ K in Figure 2B). The ac susceptibility data $\chi(T)$ are compared with the predictions of the model in Figure 8 for some of the values of the applied field. Here, the model is unable to reproduce the data at 3 and 9 T and shows smaller differences, even for $B = 1$ T (not shown). Thus, the ac susceptibility strongly depends on the deviations from the isotropic, noninteracting linear chain behavior, and the model is unable to explain the severe reduction (flattening) of the susceptibility at low temperatures and high magnetic fields.

EPR Data. *The g Factor*. The observed angular variation of the $\mathbf{g}^2$ factor was analyzed in terms of the spin Hamiltonian of eq 20 that considers the collapse of the lines produced by the exchange interaction. Because the exchange term does not affect the position of the line, the components of the crystal $\mathbf{g}^2$ tensor (defined in eq 16) were obtained from a least-squares fit of the function $g^2(\theta,\phi)=(\mathbf{h}\cdot\mathbf{g}\cdot\mathbf{g}\cdot\mathbf{h})$ to the data in Figure 5. The values of these components are given in Table 1, and the calculated values are included as solid lines in Figure 5. Information about the nondiagonal components of the molecular $\mathbf{g}$ tensors $\mathbf{g}_A$, $\mathbf{g}_B$, $\mathbf{g}_C$, and $\mathbf{g}_D$ is lost in the average. To evaluate these components, additional assumptions need to be made. We assume that the molecular $\mathbf{g}$ tensors $\mathbf{g}_A$, $\mathbf{g}_B$, $\mathbf{g}_C$, and $\mathbf{g}_D$ are diagonal in a reference system approximately determined by the directions of the ligands Cu1−O1 and Cu1−O2 (the angle O1−Cu−O2 is 89.9°) and the direction perpendicular to the copper coordination plane. This allows us to calculate the components of $\mathbf{g}_A$, $\mathbf{g}_B$, $\mathbf{g}_C$, and $\mathbf{g}_D$ and their nondiagonal elements in the crystal system determined by *a*, *b*, and *c*. Using the crystallographic information[45] for site A (see Crystal Section), we obtain the molecular

TABLE 1: Components of the Crystal g^2 Tensor Obtained from Least-Squares Fits to the EPR Single-Crystal Data at 9.5 and 35 GHz in Figure 5[a]

	9.5 GHz	35 GHz		calcd
g^2_{xx}	4.7150 (6)	4.6805 (6)	g^M_{xx}	2.1634
g^2_{yy}	4.2474 (6)	4.2394 (5)	g^M_{yy}	2.0590
g^2_{zz}	4.4040 (6)	4.3758 (5)	g^M_{zz}	2.0918
g^2_{xy}	0.0001 (8)	−0.0001 (7)	g^M_{xy}	0.0486
g^2_{zx}	−0.0001 (8)	−0.0001 (7)	g^M_{zx}	0.0918
g^2_{zy}	0.0001 (8)	0.0001 (7)	g^M_{zy}	0.0210

[a] Second and third columns. The fifth column shows the components of the molecular $\mathbf{g}$ tensor for the site A, calculated as explained in the text.

TABLE 2: Values of Parameters a_u and b_u (in 10^{-4} T) Obtained from Least-Squares Fits of Eq 25 to the Angular Variation of the Line Width Observed in a Single Crystal Sample at 9.5 and 35 GHz[a]

	9.5 GHz	35 GHz
a_1	79.9 (3)	62 (1)
a_2	130.5 (3)	142.0 (5)
a_3	59.2 (3)	56.4 (9)
b_1	$-0.221\ (9) \times 10^6$	$-0.225\ (8) \times 10^6$
b_2	$0.205\ (2) \times 10^5$	$0.335\ (2) \times 10^6$
b_3	$-0.111\ (2) \times 10^6$	$-0.174\ (2) \times 10^6$

[a] Figure 6

$\mathbf{g}$ tensor included in Table 1. The nondiagonal components of $\mathbf{g}_M$ (Table 1) along with eqs 24 allow us to calculate exchange couplings from the line width data.

Evaluation of the Exchange Parameters from the Line Width Data. The function

$$\Delta B_{pp}(\theta,\phi) = a_1 \sin^2\theta\cos^2\phi + a_2 \sin^2\theta \sin^2\phi + a_3 \cos^2\theta + \sum_{u=1}^{3} \frac{b_u(\mathbf{h}\cdot\mathbf{g}\cdot\mathbf{G}_u\cdot\mathbf{h})^2}{g^4(\theta,\phi)} \quad (25)$$

was fitted to the line width data in Figure 6. The angles θ and ϕ define the direction of $\mathbf{B}$ in the *abc* crystal axes system. The parameters a_u and b_u ($u = 1, 3$) obtained (Table 2) were used to draw the solid lines in Figure 6. The coefficients a_u account for second-order contributions as hyperfine and dipole−dipole interactions, and are approximately frequency-independent. The last term in equation eq 25 is the contribution to the line width introduced in eq 22. We relate the b_u parameters to the contribution of the residual Zeeman interaction (eq 21). Comparing eqs 22 and 25 leads to

$$b_u(\omega_o) = \sqrt{\frac{2\pi}{3}} \frac{\omega_o^2 \hbar}{g\mu_B \omega_{ex}^{(u)}} \quad (26)$$

Thus, when eq 22 is valid, one should observe

$$\frac{b_u(35\ \text{GHz})}{b_u(9.5\ \text{GHz})} \approx \left(\frac{35\ \text{GHz}}{9.5\ \text{GHz}}\right)^2 \approx 13 \quad (27)$$

Table 2 and Figure 6 show that only the parameter b_2 displays the quadratic frequency dependence predicted by eq 26. In addition, b_1 and b_3 are negative, although eq 26 predicts positive values. This is an expected result, because eq 26 is valid only when the residual Zeeman interaction is the main mechanism contributing to the line width, which is not the case for b_1 (*cb* plane) and b_3 (*ab* plane). These parameters are associated with

the exchange frequencies $\omega_{ex}^{(1)}$ and $\omega_{ex}^{(3)}$, which in turn are proportional to the large intrachain exchange interaction $J = J^{(A,C)}$, a fact that makes the residual Zeeman negligible in those planes (see Figure 6A,C). Meanwhile, b_2 is inversely proportional to $\omega_{ex}^{(2)}$, which depends on the much smaller interchain interactions. Furthermore, even at 35 GHz, fourth-order terms arising from dipole−dipole interactions contribute to the line width in the *ab* and *cb* planes. At 9.5 GHz, these contributions increase, and the uncertainties of b_1 and b_3 are large. Using eq 26 and the value of b_2 at 35 GHz (Table 2), we evaluated $\omega_{ex}^{(2)} = 1.13 \times 10^{10}$ s^{-1}. Thus, from eq 23a

$$[(2J^{(A,B)})^2 + (2J^{(A,D)})^2]^{1/2}/k = 0.061(2) \text{ K}$$

Discussion and Conclusions

Here we discuss the results of our work from two different points of view. The magnitudes of the evaluated intra- and interchain exchange interactions are discussed in terms of the structural information on Cu(II)Trp-Gly[29] and previous magnetic studies in similar chains. Then we discuss the magnetic behavior and its deviations from what is expected for ferromagnetic chains.

Magnitudes of the Exchange Interactions. *The Intrachain Exchange Interactions.* Our magnetic susceptibility and magnetization data reflect the FM character of the copper chains. The value $2J/k = (3.9 \pm 0.1)$ K obtained for the intrachain interaction should be compared with the values reported previously for similar helical copper chains coupled by syn−anti carboxylate bridges. Carlin et al.[8] studied the compound $[Cu(NH_3)_2(CH_3COO)Br]$ in which the copper ions are in zigzag chains connected by asymmetric acetate bridges. At high temperature, the specific heat and susceptibility data were explained with an AFM intrachain coupling $2J/k = -8.6$ K. Considering the deviations of the data below 10 K from the values expected for a linear chain, they calculated an unexpectedly large interchain interaction $zJ'/k = -1.9$ K. In addition, a three-dimensional phase transition is observed at 4.146 K. The large interchain interactions, attributed to the hydrogen-bonding network linking the chains, would be responsible for the relatively high transition temperature. A similar AFM behavior was observed by Nanda et al.[12] for the helical spin chains found in a Cu(II)−thioether carboxylate complex. Colacio et al.[10] reported a structural and magnetic study of a quasi-tetrahedral Cu_4 cluster, bridged as a ring by syn−anti carboxylate bridges. The behavior of this complex is FM, and the authors calculate $2J/k = 6.8$ K using the hypothesis that all of the exchange couplings within the 4-ion clusters are the same. In more recent papers, Colacio et al.[10,15,16] also reported structural and magnetic studies of several linear chain Cu compounds in which the intrachain bridges are syn−anti carboxylate bridges, and the coupling is FM. These chains and the geometry of the bonds between ligand and metal ion are very similar to what it is found for Cu(II)Trp-Gly. These authors attribute the FM coupling between copper ions in these compounds to a very small value of the AFM contribution, produced by a negligible overlap between the magnetic orbitals corresponding to neighbor coppers in the chains.[51] This occurs because 2p orbitals from the oxygen ions are unfavorably oriented in the syn−anti carboxylate bridges. This qualitative explanation accounts for the FM behavior observed by us in Cu(II)Trp-Gly; however, we did not find a quantitative correlation between the magnitude of the interaction and the distances and angles of the Cu−O−C−O−Cu bridge or the deviations of the copper ions from the plane defined by the carboxylate bridge. Thus, a detailed quantitative analysis of the magnitudes of the exchange in terms of structural parameters still demands theoretical work.

The Interchain Exchange Interactions. We prove here that exchange interactions can be transmitted through cation−π contacts between the copper(II) ion and the indole ring of the amino acid. The magnitude of this interaction is small ($[(2J^{(A,B)})^2 + (2J^{(A,D)})^2]^{1/2}/k = 0.061$ K), is obtained from the EPR line width data via a method independent of the magnetic measurements, and is used to evaluate the intrachain interaction. This method does not provide the sign of the interaction. On the basis of the structural data, we assume that the interaction $J^{(A,D)}$ supported by the A−D cation−π contact is stronger than the interaction $J^{(A,B)}$ supported by the A−B cation−π contact. Under this assumption we obtained

$$|2J^{(A,D)}/k| \approx |2J'/k| \approx 0.061 \text{ K}$$

The order of magnitude of this interaction is similar to what it is observed for long superexchange paths involving hydrogen bonds,[32] with similar total lengths. They are also found in cases when the two magnetic orbitals are connected by the stacking of aromatic rings belonging to the magnetic orbitals of the metal ions.[29] The magnitudes of the exchange couplings transmitted by long noncovalent bonds with small electron densities are weakly dependent on the details of the bonds and can be described[53,54] by empirical rules that give the order of magnitude of the interaction. This is similar to what has been done to calculate the maximum electron-transfer rate between redox centers in biological structures[55] and makes more interesting measuring exchange interactions transmitted by long paths in biological molecules. Their theoretical calculations are not possible nowadays. Thus, a better knowledge of these empirical rules in model systems with biologically relevant superexchange bridges may be helpful to learn about the electron-transfer rates.[34]

Deviations of the Magnetic Behavior from What Is Expected for an FM Chain. We attribute the deviations of the ac susceptibility data with applied dc magnetic field from the predictions of the linear chain models observed in Figure 8 to anisotropy of the intrachain interaction J_{ac} (not considered in eq 4) and to interchain interactions. Our data strongly suggests the properties of CHAC (cyclohexylammonium copper trichloride), a compound studied in great detail several years ago,[20,56,57] and other similar systems, as well. The main characteristic of that material is the presence of strongly coupled FM chains along the *c* axis ($J_1/k = +70$ K), which defines a preferred direction. These chains are weakly coupled to other chains within the *bc* plane ($J_2 \approx 10^{-3}J_1$, also FM) and interact with other chains in the *ac* plane via even weaker AFM interactions ($|J_3| \approx 10^{-4}|J_1|$). The magnetic anisotropy introduced by the interchain exchange couplings produces strong effects on the magnetization curves and on the FM resonance spectrum. A detailed analysis of these effects requires magnetic measurements in single-crystal samples and is out of the scope of this work; however, our results indicate interesting metamagnetic properties of Cu(II)Trp-Gly that remain to be studied. We show that the ac susceptibility measurements with applied dc magnetic fields offer a very sensitive measurement method. Meanwhile, the magnetic susceptibility measured with no dc magnetic field is very well explained using the models. The fact that the *g* value obtained from the saturation magnetization (2.07) is about 1.5% larger than that calculated from the susceptibility data (2.04) in the same sample would indicate a canting of the spins of the copper ions in the chains, which is expected from structural considerations.

Acknowledgment. The authors acknowledge financial support from FAPESP, CNPq, and CAPES in Brazil and CONICET and CAI+D-UNL in Argentina. Multinational grants of Antorchas and Vitae Foundations made this collaboration possible. RC is a member of CONICET.

References and Notes

(1) Bleaney, B.; Bowers, K. D. *Proc. R. Soc. London A* **1952**, *214*, 451.
(2) van Niekerk, J. N.; Schoening, F. R. L. *Acta Crystallogr*. **1953**, *6*, 227.
(3) Güdel, H. U.; Stebler, A.; Furrer, A. *Inorg. Chem*. **1979**, *18*, 1021.
(4) Carlin, R. *Magnetochemistry*; Springer: Berlin, 1985.
(5) Kahn, O. *Molecular Magnetism*; VCH: New York, 1993.
(6) Weder, J. E.; Hambley, W. H.; Kennedy, B. J.; Lay, P. A.; MacLachlan, D.; Bramley, R.; Delfs, C. D.; Murray, K. S.; Moubaraki, B.; Warwick, B.; Biffin, J. R.; Regtop, H. L. *Inorg. Chem*. **1999**, *38*, 1736.
(7) Schlam, R. F.; Perec, M.; Calvo, R.; Lezama, L.; Insausti, M.; Rojo, T.; Foxman, B. M. *Inorg. Chim. Acta* **2001**, *310*, 81.
(8) Carlin, R. L.; Kopinga, K.; Kahn, O.; Verdaguer, M. *Inorg. Chem.* **1986**, *25*, 1786.
(9) Levstein, P. R.; Calvo, R. *Inorg. Chem*. **1990**, *29*, 1581.
(10) Colacio, E.; Costes, J. P.; Kivekas, R.; Laurent, J. P.; Ruiz, J. *Inorg. Chem*. **1990**, *29*, 4240.
(11) Colacio, E.; Dominguez-Vera, J. M.; Costes, J. P.; Kivekäs, R.; Laurent, J. P.; Ruiz, J.; Sundberg, M. *Inorg. Chem.* **1992**, *31*, 774.
(12) Nanda, K. K.; Addison, A. W.; Sinn, E.; Thompson, L. K. *Inorg. Chem*. **1996**, *35*, 5996.
(13) Schulz, D.; Weyhermüller, T.; Wieghartdt, K.; Butzlaff, C.; Trautwein, A. X. *Inorg. Chim. Acta* **1997**, *247*, 387.
(14) Cheng, P.; Liao, D.; Yan, S.; Jiang, Z.; Wang, G.; Yaop, X.; Wang, H. *Inorg. Chim. Acta* **1997**, *254*, 371.
(15) Colacio, E.; Ghazi, M.; Kivekäs, R.; Moreno, J. M. *Inorg. Chem.* **2000**, *39*, 2882
(16) Colacio, E.; Dominguez-Vera, J. M.; Ghazi, M.; Kivekäs, R.; Klinga, M.; Moreno, J. M. *Eur. J. Inorg. Chem.* **1999**, 441.
(17) Que, L., Jr.; True, A. *Prog. Inorg. Chem*. **1990**, *38*, 97.
(18) Bonner, J. C.; Fisher, M. E. *Phys. Rev*. **1964**, *135A*, 640.
(19) Baker, G. A. Jr.; Rushbrooke, G. S.; Gilbert, H. E. *Phys. Rev*. **1964**, *135A*, 1272.
(20) Willet, R. D.; Gaura, R. M.; Landee, C. P. In *Extended Linear Chain Compounds*; Miller, J. S., Ed.; Plenum: New York, 1983; Vol. 3.
(21) Willet, R. D.; Landee, C. P. *J. Appl. Phys.* **1981**, *52*, 2004.
(22) Steiner, M.; Villain, J.; Windsor, G. G. *Adv. Phys*. **1976**, *25*, 87.
(23) Steiner, M. *J. Appl. Phys.* **1979**, *50*, 7395.
(24) Perutz, M. F. *Philos. Trans. R. Soc. A* **1997**, *345*, 105.
(25) Jeffrey, G. A.; Saenger, W. *Hydrogen Bonding in Biological Structures*; Springer: Berlin, 1991.
(26) Jeffrey, G. A. *An Introduction to Hydrogen Bonding*; Oxford: New York, 1997.
(27) Fisher, B. E.; Sigel, H. *J. Am. Chem. Soc.* **1980**, *102*, 2998.
(28) Sugimori, T.; Shibakawa, K.; Masuda, H.; Odani, A.; Yamauchi, O. *Inorg. Chem*. **1993**, *32*, 4951.
(29) Costa-Filho, A. J.; Munte, C. E.; Barberato, C.; Castellano, E. E.; Mattioli, M. P. D.; Calvo, R.; Nascimento, O. R. *Inorg. Chem*. **1999**, *38*, 4413.
(30) Dougherty, D. A. *Science* **1996**, *271*, 163.
(31) Ma, J. C.; Dougherty, D. A. *Chem. Rev.* **1997**, *97*, 1303.
(32) Ryzhov, V.; Dunbar, R. C. *J. Am. Chem. Soc.* **1999**, *121*, 2259.
(33) This definition of J follows classical papers on spin chains (refs 18, 19) and is different from that often used nowadays ($-J_{ij}S_iS_j$, see ref 5). For the sake of uniformity in this paper, we use eq 1 for all exchange interactions.
(34) Calvo, R.; Abresch, E.; Bittl, W.; Feher, G.; Hofbauer, W.; Isaacson, R. A.; Lubitz, W.; Okamura, M. Y.; Paddock, M. L. *J. Am. Chem. Soc.* **2000**, *122*, 7327.
(35) Brill, A. S. *Transition Metals in Biochemistry*; Springer: Berlin, 1977.
(36) Lippard, S. J.; Berg, J. M. *Principles of Bioinorganic Chemistry*; University Science Books: Mill Valley, CA, 1994.
(37) Levstein, P. R.; Calvo, R.; Castellano, E. E.; Piro, O. E.; Rivero, B. E. *Inorg. Chem*. **1990**, *29*, 3918.
(38) Calvo, R.; Passeggi, M. C. G.; Novak, M. A.; Symko, O. G.; Oseroff, S. B.; Nascimento, O. R.; Terrile, M. C. *Phys. Rev. B* **1991**, *43*, 1074.
(39) Brondino, C. D.; Casado, N. M. C.; Passeggi, M. C. G.; Calvo, R. *Inorg. Chem*. **1993**, *32*, 2078.
(40) Siqueira, M. L.; Rapp, R. E.; Calvo, R. *Phys. Rev. B* **1993**, *48*, 3257.
(41) Rapp, R. E.; de Souza, E. P.; Godfrin, H.; Calvo, R, *J. Phys.: Condens. Matter* **1995**, *7*, 9595.
(42) Martino, D.; Passeggi, M. C. G.; Calvo, R. *Phys. Rev. B* **1995**, *52*, 9466.
(43) Martino, D. M.; Passeggi, M. C. G.; Calvo, R.; Nascimento, O. R. *Physica B* **1996**, *225*, 63.
(44) Calvo, R.; Passeggi, M. C. G.; Moreno, N. O.; Barberis, G. E.; Braun-Chaves, A.; Torres, B. C. M.; Lezama, L.; Rojo, T. *Phys. Rev. B* **1999**, *60*, 1197.
(45) Nascimento, O. R.; Costa-Filho, A. J.; De Morais, D. I.; Ellena, J.; Delboni, L. F. *Inorg. Chim. Acta* **2001**, *312*, 133.
(46) Kozlowski, H. *Chem. Phys. Lett.* **1977**, *46*, 519.
(47) Anderson, P. W. *J. Phys. Soc. Jpn.* **1954**, *9*, 316.
(48) Kubo, R.; Tomita, K. *J. Phys. Soc. Jpn.* **1954**, *9*, 888.
(49) Passeggi, M. C. G.; Calvo, R. *J. Magn. Res. A* **1995**, *114*, 1.
(50) *International Tables for X-ray Crystallography*, 2nd ed.; Hahn, T., Ed.; Reidel: Dordrecht, 1987; Vol. 2. We follow the definition of symmetry-related positions given in this edition of the Table.
(51) Hay, P. J.; Thibeault, R. H.; Hoffmann, R. H. *J. Am. Chem. Soc.* **1975**, *97*, 4884.
(52) Sartori, R. P.; Ortigoza, L.; Casado, N. M. C.; Calvo, R.; Castellano, E. E.; Piro, O. E. *Inorg. Chem.* **1999**, *38*, 3598.
(53) Coffman, R. E.; Buettner, G. R. *J. Phys. Chem*. **1979**, *83*, 2387.
(54) Hoffmann, S. K.; Hilczer, W.; Gozlar, J. *J. Appl. Magn. Reson*. **1994**, *7*, 289.
(55) Moser, C. C.; Keske, J. M.; Warncke, K.; Farid, R. S.; Dutton, P. L. *Nature* **1992**, *355*, 796.
(56) Willet, R. D.; Landee, C. P.; Gaura, R. M.; Swanck, D. D.; Groenendijk, H. A.; van Duyneveldt, A. J. *J. Magn. Magn. Mater*. **1980**, *15−18*, 1055.
(57) Groenendijk, H. A.; van Duyneveldt, A. J.; Blöte, H. W. J.; Gaura, R. M.; Landee, C. P.; Willet, R. D. *Physica* **1981**, *106B*, 47.